Why non-heme iron halogenases do not fluorinate C-H bonds: a computational investigation

Vyshnavi Vennelakanti[1,2], Grace L. Li[1], and Heather J. Kulik[1,2]*

[1]*Department of Chemical Engineering, Massachusetts Institute of Technology, Cambridge, MA 02139*

[2]*Department of Chemistry, Massachusetts Institute of Technology, Cambridge, MA 02139*

ABSTRACT: Selective halogenation is necessary for a range of fine chemical applications including the development of therapeutic drugs. While synthetic processes to achieve C–H halogenation require harsh conditions, enzymes such as non-heme iron halogenases carry out some types of C–H halogenation, i.e., chlorination or bromination, with ease while others, i.e., fluorination, have never been observed in natural or engineered non-heme iron enzymes. Using density functional theory and correlated wavefunction theory, we investigate the differences in structural and energetic preferences of the smaller fluoride and the larger chloride or bromide intermediates throughout the catalytic cycle. Although we find that the energetics of rate-limiting hydrogen atom transfer are not strongly impacted by fluoride substitution, the higher barriers observed during the radical rebound reaction for fluoride relative to chloride/bromide contribute to the difficulty of C–H fluorination. We also investigate the possibility of isomerization playing a role in differences in reaction selectivity, and our calculations reveal crucial differences in terms of isomer energetics of the key ferryl intermediate between fluoride and chloride/bromide intermediates. While chloride and bromide intermediates show formation of monodentate isomers believed to be involved in selective catalysis, we find that formation of the fluoride monodentate intermediate is not possible in our calculations that lack additional stabilizing interactions with the greater protein environment. Furthermore, the shorter Fe–F bonds are found to increase isomerization reaction barriers, suggesting that incorporation of residues that form a halogen bond with F and elongate Fe–F bonds could make selective C–H fluorination possible in non-heme iron halogenases. Our work highlights the differences between the fluoride and chloride/bromide intermediates and suggests potential steps towards engineering non-heme iron halogenases to enable selective C–H fluorination.

1. Introduction.

The selective functionalization[1-6] of unactivated C–H bonds remains one of the greatest challenges in catalysis. Inspiration can be taken from nature, where selective enzymatic C–H halogenation plays a critical role in numerous biochemical processes.[7, 8] In addition to their incorporation in natural products[9-11] and related biological[7, 12, 13] and medicinal[14-16] applications, halogenated compounds find a wide variety of uses in therapeutic drugs[17-19] and agrochemicals.[20-22] The enzymes that carry out C–H activation are typically α-ketoglutarate (αKG)-dependent enzymes that operate under ambient conditions with strong regioselectivity and stereoselectivity[23] resulting in the catalysis of a wide variety of reactions[24-27], including halogenation. For non-heme iron halogenases in particular[28-30], e.g., SyrB2[31, 32], CytC3[33, 34], WelO5[35], and BesD,[36] the active sites are similar to other non-heme iron enzymes with only one major change. In comparison to more well understood non-heme iron hydroxylases,[37-39] the halogenases have a halide coordinating the metal center, i.e., native chloride or non-native bromide. This halide is bound in place of a carboxylate of the 2-His-1-carboxylate facial triad of the hydroxylases[40-42] because in the halogenases there is no carboxylate-bearing aspartate or glutamate residue present and instead a non-coordinating alanine residue is typically present to create a hydrophobic pocket for halide binding. Despite this understanding of halogenases, it is extremely hard[43] to develop selective processes for C–H halogenation using synthetic methods due to the inertness[44] of C–H bonds and their high bond dissociation energy.

Non-heme iron halogenases natively carry out C–H chlorination[28, 32, 35], and C–H bromination has been observed *in vitro* in SyrB2 but with lower efficiency[23, 45] than chlorination. This is corroborated by the abundance[13, 46, 47] of chlorinated and brominated natural products. On the contrary, C–H fluorination has never been observed[23, 46, 48, 49] in any of the non-heme iron

halogenases. Recent work on an engineered enzyme SadX in which fluoride was incorporated into the active site showed that the enzyme could hydroxylate but not fluorinate substrates.[50] Additionally, a recent computational and experimental study[51] on hydroxylation versus halogenation in mononuclear nonheme iron complexes showed that while computational results predict substrate fluorination to be feasible, attempts to synthesize the Fe(III)-OH intermediate with fluoride in the active site have been unsuccessful. Selective C–H fluorination is desired for the development of fine chemicals, i.e., in the pharmaceutical industry,[52-55] thus understanding how we can make C–H fluorination possible in halogenases could help with the synthesis of fluorinated drugs. Because fluorination by non-heme halogenases is not observed in nature, re-engineering of biological systems to enable C–F bond formation would be of great use.

C–H chlorination by non-heme iron halogenases has been extensively studied through experiments[27, 56, 57] and computation[58-61] with fewer studies of C–H bromination[32, 45, 62] and fluorination[50, 51] having been carried out. The only enzyme with fluorinase activity characterized to date uses a mechanism entirely distinct from the radical rebound mechanism[63] from non-heme iron halogenases. This enzyme, 5'-fluoro-5'-deoxyadenosine synthase[23, 46, 64-67], is a nucleophilic halogenase, the mechanism of which involves fluoride attack on an electrophilic carbon through an S_N2-type displacement reaction[68-70] . Fluorine sits in a small-sized hydrophobic binding pocket in these enzymes, and it has been hypothesized that while a larger binding pocket makes chlorination, bromination, and iodination of nucleophilic halogenases possible, it eliminates their fluorination activity.[23] Prior studies[22, 46, 48] suggest that strong electronegativity of fluorine combined with the large enthalpic cost of fluoride desolvation[71] and its toxicity[72] could explain why biological C–H fluorination by non-heme iron halogenases has never been observed. However, no prior computational or experimental work has studied the influence of the halogen

identity on C–H halogenation by non-heme iron halogenases.

In this work, we compare and contrast C–H halogenation carried out by the active site of non-heme iron halogenases using three halides: fluoride, chloride, and bromide. We study the rate-determining hydrogen atom transfer (HAT) and rebound reactions to determine if these reaction barriers could explain why C–H chlorination and bromination are preferred over C–H fluorination. Because isomerization to alter relative substrate positioning[58, 60, 73-76] has been invoked to rationalize selectivity of some[35, 58, 59, 75] albeit not all[60, 74] non-heme iron halogenases, we also study isomer energetics and isomerization reaction coordinates (RCs) to understand the isomer energetic favorability of key intermediates such as Fe(IV)=O and Fe(III)-OH formed during the catalytic cycle with all three halides.

2. Computational Details.

The active site of WelO5[35, 77, 78] (PDBID: 5IQS), a representative, carrier-protein-free non-heme iron halogenase, was extracted from the enzyme's crystal structure, following the protocol from prior work.[61] The native halide, i.e., chloride, was replaced with fluoride and bromide to generate three active site models corresponding to the three halides (Supporting Information Figure S1). Active site intermediates and corresponding isomers of these active site models containing water (i.e., as in the crystal structure), O_2, oxo, hydroxo, and succinate (monodentate and bidentate) ligands were generated by modifying the crystal structure with molSimplify,[79] which uses OpenBabel[80, 81] as a backend. Consistent with prior work,[61] the metal-distal carboxylate oxygen of αKG and succinate ligands along with Nδ atoms of His ligands were protonated using Avogadro v1.2.0[82] to ensure an overall neutral charge for the final active site models (Supporting

Information Figure S1). All hydrogen atoms added to the active site models were force-field optimized in Avogadro with the UFF[83] force field while holding the heavy atoms fixed.

All geometry optimizations were carried out in ORCA[84] v.4.0.1.2 and v.4.2.1 using density functional theory (DFT) with the generalized gradient approximation (GGA) global hybrid PBE0[85] and the def2-TZVP basis set[86] and employing semi-empirical D3[87] dispersion with Becke-Johnson[88] damping. The resolution of the identity (RI) approximation[89-93] was used, and the auxiliary basis set for def2-TZVP was generated automatically[94] by ORCA to accelerate calculations. Consistent with prior work[61], the five heavy atoms of succinate and the methyl carbon atoms of His ligands were held fixed to mimic the ligand positions in the enzyme (Supporting Information Figure S2). Optimizations were performed in the gas phase and in solution using the BFGS algorithm in redundant internal coordinates. The default thresholds of 5×10^{-6} hartree for the change in self-consistent field (SCF) energy between steps and 3×10^{-4} hartree/bohr for the maximum gradient were used. The solution calculations were carried out using the conductor-like polarizable continuum model[95] (C-PCM) solvation energies along with the conductor-like screening solvent model (COSMO) epsilon function type. A solvent dielectric value of $\varepsilon = 10$ was used, approximately mimicking the protein environment. As observed in prior work[61], we find that the inclusion of environment effects through implicit solvent alters most gas-phase geometries very little (i.e., most are within 0.01–0.03 Å while a few outliers have larger changes), thus we carry out further analyses only in the gas phase (Supporting Information Table S1). Low-spin (LS) singlet states were simulated in a spin-restricted formalism while non-singlet LS doublet, intermediate-spin (IS), and high-spin (HS) states were simulated in an unrestricted formalism (Supporting Information Table S2). All initial and optimized structures for gas-phase and implicitly solvated optimizations are provided in the Supporting Information.

Reaction coordinates (RCs) for isomerization of axial to equatorial (i.e., of oxo/hydroxo/halide ligands) were obtained using the protocol from prior work[61] at the PBE0-D3/def2-TZVP level of theory. These RCs were sampled by rotating the oxo/hydroxo/halide ligand with respect to the axial His in 1° increments of the angle formed by the ligand, the Fe center, and nitrogen of the axial His from 90° to 180° (Supporting Information Figure S2). Reaction coordinates for hydrogen atom transfer (HAT) and radical rebound were obtained at the B3LYP-D3/6-31G* level of theory. The B3LYP/6-31G* method/basis set combination was chosen to reduce the computational cost associated with the larger def2-TZVP basis set due to increased system size from the presence of substrate atoms in these calculations and for consistency with prior work.[50, 61] Hydrogen atom transfer (HAT) RCs were obtained using Fe(IV)=O and lysine, which is the substrate of a representative non-heme iron halogenase, BesD[36]. The radical rebound RCs (i.e., with both hydroxo and halogen F, Cl, or Br) were modeled following prior work[50] as the rebound of a 2-methylbutane radical to an Fe(III)–OH intermediate, where 2-methylbutane was chosen as the model substrate because it closely resembles most substrates of Fe(II)/αKG-dependent enzymes (Supporting Information Figure S2).

The five heavy atoms of succinate and the methyl carbon atoms of His ligands were constrained in isomerization, radical rebound, and HAT RCs (Supporting Information Figure S2). Additionally, the relevant RC angles were constrained in isomerization RCs (Supporting Information Figure S2). Heavy atoms of the lysine substrate and the distance between the oxo ligand and the relevant hydrogen atom of lysine were also constrained and varied in increments of 0.05 Å for HAT RCs (Supporting Information Figure S2). For rebound RCs, the distance between the carbon radical of the model substrate and oxygen of OH or halide was constrained and varied in increments of 0.1 Å (Supporting Information Figure S2). High-energy structures along all RCs

were used to obtain vibrational frequencies using gas-phase numerical Hessian calculations carried out at the corresponding levels of theory. The Hessian was computed using the central difference approach after 6*N* atomic displacements. The presence of an imaginary frequency along the RC confirmed characterization of high-energy structures along the RCs as transition states.

Single-point energy calculations on the optimized geometries of active-site intermediates and their isomers were performed using domain-localized pair natural orbital coupled cluster with singles, doubles and perturbative triples (i.e., DLPNO-CCSD(T)[96, 97]) in ORCA v4.0.1.2. Two-point[98-100] extrapolation to the complete basis set (CBS) limit was carried out using Dunning-style correlation-consistent double-ζ and triple-ζ (i.e., aug-cc-pVDZ and aug-cc-pVTZ) basis sets. All reported DLPNO-CCSD(T)/CBS energies were obtained using tight PNO thresholds, consistent with prior work[61] (Supporting Information Table S3). Mayer bond order analysis to quantify the strength of binding of αKG, monodentate, and bidentate succinate ligands to iron was performed using Multiwfn[101].

3. Reaction Mechanism.

Prior work based on the crystal structures[32, 35, 36] and spectroscopic studies[33, 102] of non-heme iron halogenases along with the related non-heme iron dioxygenases[24, 27, 40, 103] and hydroxylases[33, 104] has led to the proposal of the following mechanism[24, 27, 32, 33, 48] in the catalytic cycle for non-heme iron halogenases. In its resting state (**1**), the hexa-coordinated iron active site consists of an Fe(II) coordinated to two His ligands, a bidentate αKG ligand, a halide ligand, and a water molecule, which is loosely bound to the iron center (Figure 1). When the substrate enters the binding pocket in the active site, the water molecule is displaced, followed by the binding of molecular oxygen (**2**) to the iron center (Figure 1). The bound molecular oxygen immediately

attacks the carbonyl carbon of the bidentate αKG ligand, leading to O–O bond cleavage and oxidative decarboxylation of αKG (Figure 1). During this catalytic step, the decarboxylation of an initially bidentate coordinating αKG leads to release of a carbon dioxide molecule, leaving behind succinate that has a carboxylate group that can bind iron in a monodentate or bidentate fashion (Figure 1). This conversion leads to the appearance of an active site consisting of a highly reactive terminal Fe(IV)-oxo intermediate (**3**), which abstracts a hydrogen atom from the substrate, forming a radical substrate and an Fe(III)–OH intermediate (**4**) (Figure 1). This rate-determining HAT step is followed by rebound halogenation of the substrate radical by the halide ligand, which returns the active site to its resting state (**1**) (Figure 1). We assume that the Fe(IV)=O intermediate can form after oxidative decarboxylation based on our prior study of an engineered SadX enzyme with fluoride and chloride bound, where both could form hydroxylated products, and therefore the Fe-oxo intermediate must have formed, but only the chloride bound active site led to chlorinated products.[50] Thus, we focus on the HAT and rebound steps (i.e., **3** and **4**), and we study this mechanism for three halides: fluoride, chloride, and bromide.

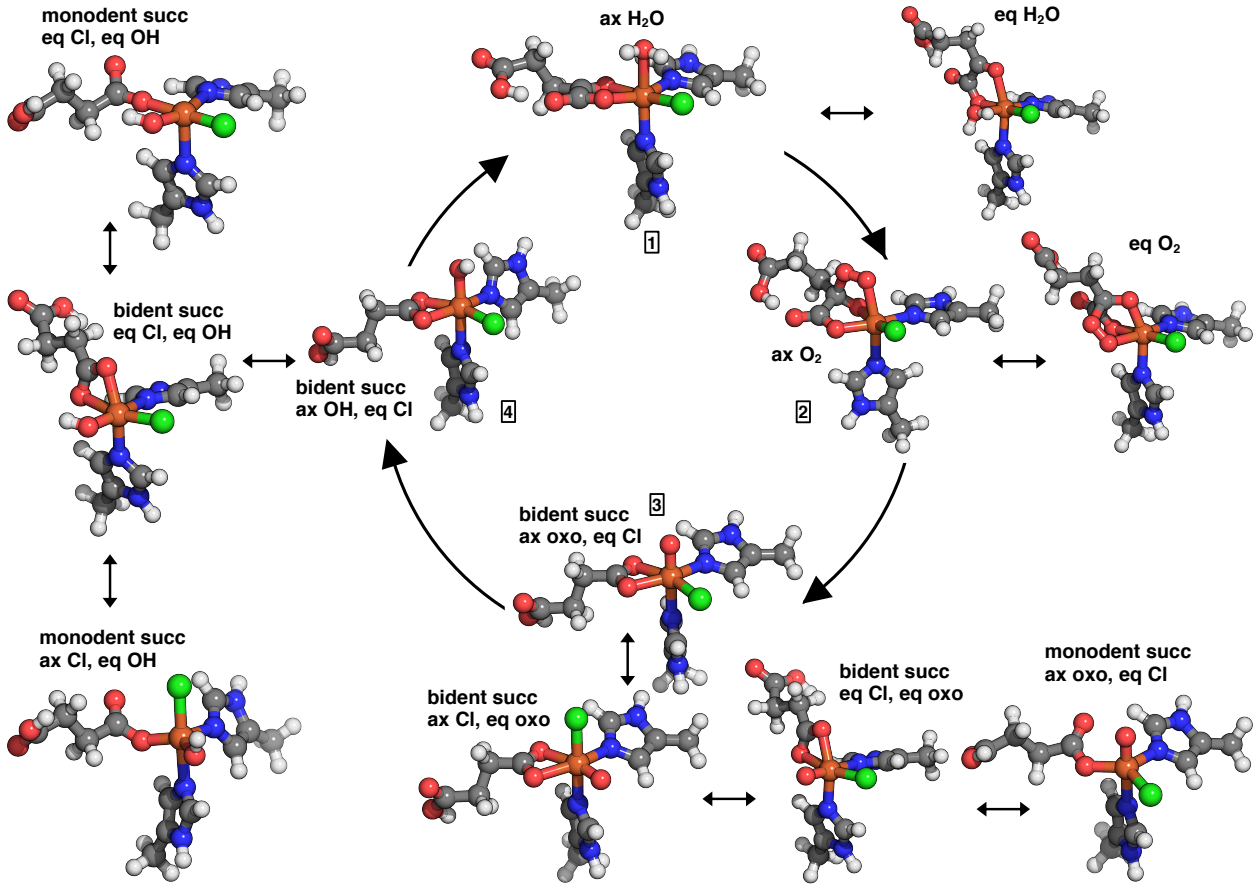

Figure 1. Proposed reaction mechanism of non-heme iron halogenases (clockwise from the top): the intermediates with water loosely bound to the iron center (**1**); O_2 bound to the iron center (**2**); oxo and succinate (**3**); and hydroxo bound to iron (**4**) are shown with representative isomers of chloride intermediates. Fe(II)–H_2O and Fe(III)–O_2 each have two isomers: axial (ax) and equatorial (eq) H_2O/O_2. Fe(IV)=O and Fe(III)–OH intermediates each have six isomers: (i) bidentate (bident.) succinate (succ.), axial oxo/OH, equatorial chloride (ii) bidentate succinate, axial chloride, equatorial oxo/OH (iii) bidentate succinate, equatorial oxo/OH, chloride (iv) monodentate (monodent.) succinate axial oxo/OH, equatorial chloride (v) monodentate succinate axial chloride, equatorial oxo/OH (vi) monodentate succinate equatorial oxo/OH, chloride. Hydrogen, carbon, nitrogen, oxygen, chlorine, and iron atoms are shown in white, gray, blue, red, green, and brown, respectively.

All the intermediates formed during the catalytic cycle can potentially exist in two or more isomers. For example, in intermediates (**1**) and (**2**), water and molecular oxygen are represented in axial positions corresponding to their respective axial configurational isomers due to the frequency with which water is found in the axial position in crystal structures of halogenases[32, 35, 36, 45] (Figure

1). However, these intermediates can also have water and molecular oxygen present in equatorial positions, corresponding to equatorial configurational isomers (Figure 1 and Supporting Information Figure S3). In the Fe(IV)=O and Fe(III)–OH intermediates, the active site can be hexa-coordinated or penta-coordinated depending on whether succinate is coordinated to iron in a bidentate or monodentate configuration (Figure 1 and Supporting Information Figure S3). In the case of a hexa-coordinated iron active site with bidentate succinate, oxo or hydroxo moieties and the halide ligand can be present in axial or equatorial positions, resulting in three configurational isomers: axial oxo/hydroxo and equatorial halide, equatorial oxo/hydroxo and axial halide, and equatorial oxo/hydroxo and halide (Figure 1 and Supporting Information Figure S3). These three configurational isomers can also be observed when we have a penta-coordinated iron active site with monodentate succinate (Figure 1 and Supporting Information Figure S3). Combining the monodentate and bidentate succinate coordination cases, we potentially have a total of six configurational isomers for intermediates (**3**) and (**4**) (Figure 1 and Supporting Information Figure S3). Along with computing reaction coordinates, we will evaluate the properties and energetics for interconversion of all of these isomers to identify which ones are most likely present during catalysis.

4. Results and Discussion.

4.1. Isomers of Intermediates for Candidate Models of Halogenases.

It is known that fluoride-bound halogenase variants of the engineered enzyme SadX solely hydroxylate, whereas chloride-bound variants can both chlorinate and hydroxylate substrates[50], but the lack of strong differences in energetics we previously identified[50] and further expand upon this work motivates investigation into alternative explanations for this difference in reactivity. For

example, isomerization has been invoked to rationalize selectivity of some[35, 58, 59, 75] albeit not all[60, 74] non-heme iron halogenases. In the cases where it has been motivated, such as cases like WelO5 where the substrate in the active site would be distant from the donating halogen in the absence of isomerization[35], isomerization of the active site after high-valent metal-oxo formation has been suggested as a key factor in the selective C–H halogenation carried out by non-heme Fe(II) enzymes[56, 105]. In particular, prior experimental[35, 56, 57, 105] and computational[58, 59, 61, 74] studies suggested that the key intermediates formed during the catalytic cycle, i.e., Fe(IV)=O and Fe(III)–OH, could isomerize to favor selective halogenation over hydroxylation by positioning the rebounding substrate radical closer to the halogen. While the relative favorability of Fe(IV)=O and Fe(III)–OH isomers in chloride intermediates has been investigated in prior studies,[61, 74] it is not known whether other halogen species exhibit different preferences. Therefore, to identify the ground spin states and to understand the relative energetics and stabilities of isomers of Fe(IV)=O and Fe(III)–OH intermediates, we study active site models of these intermediates and their isomers across all three halides, i.e., fluoride, chloride, and bromide, in all possible spin states (Supporting Information Table S2 and Figure S3). Across all halides, we find that all isomers of both studied intermediates have HS ground states (Supporting Information Table S4). Furthermore, the HS state is strongly preferred over IS and LS states for all species, and the HS ground states have longer bonds in most intermediates in comparison to the LS states (Supporting Information Tables S4–S5).

Examination of Fe(IV)=O isomers in the HS state reveals that all bidentate succinate isomers are comparable in energy and more favorable than the monodentate succinate isomers by ca. 3 kcal/mol for intermediates containing fluoride and chloride (Figure 2 and Supporting Information Table S6 and Figure S4). The monodentate succinate isomer with fluoride in the active

site was obtained using additional constraints on Fe and oxygen atoms of succinate to ensure monodentate coordination. In the absence of these constraints, this monodentate isomer optimizes to a bidentate succinate isomer, indicating that for fluoride intermediates, interactions with the greater protein environment, such as a hydrogen bond to either the proximal or distal succinate carboxylate groups that would pull the co-substrate away from iron, are likely necessary to facilitate monodentate succinate coordination. In contrast, for bromide intermediates, the monodentate succinate isomer is more favorable than two bidentate succinate isomers by ca. 1–2 kcal/mol (Figure 2). We find that the most stable Fe(IV)=O isomer is different for each halogen element (Figure 2). However, the range of relative isomer energetics is consistent, i.e., for a given halide, all isomers differ in energy by less than 3.5 kcal/mol, suggesting that isomerization of Fe(IV)=O is feasible for all halides (Figure 2 and Supporting Information Table S6 and Figure S4).

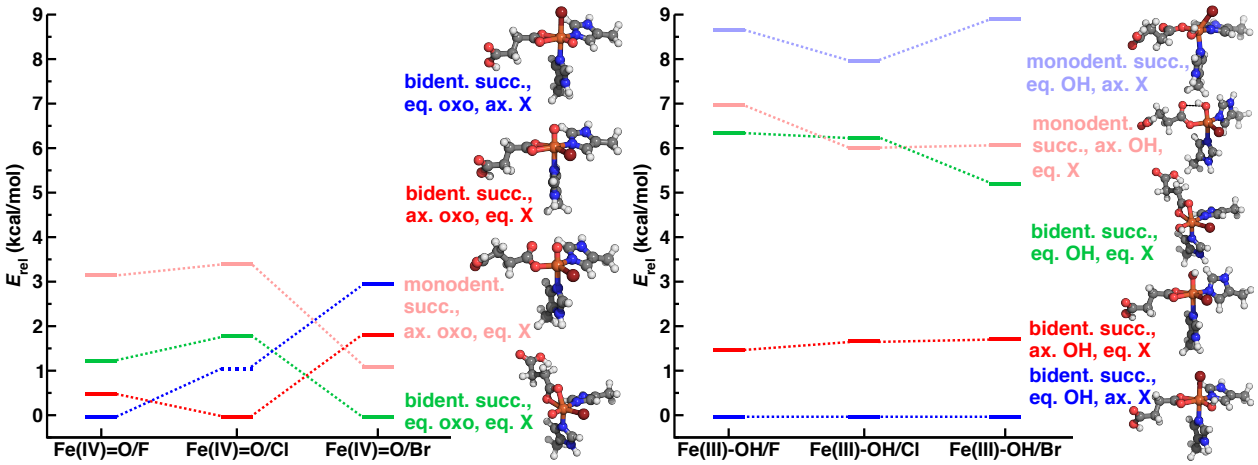

Figure 2. DLPNO/CBS energies (E_{rel}) of isomers of (left) Fe(IV)═O and (right) Fe(III)–OH intermediates shown relative to the most stable isomer for each intermediate across three halides, X = F, Cl, Br. Representative structures of Fe(IV)═O and Fe(III)–OH isomers of Br intermediates are shown in the insets and labeled. (Top to bottom, left) Isomers are equatorial (eq.) oxo, axial (ax.) X, bidentate (bident.) succinate (succ.); axial oxo and equatorial X, bidentate succinate; axial oxo, equatorial X, monodentate (monodent.) succinate; equatorial oxo and X, bidentate succinate. (Top to bottom, right) Isomers are equatorial OH, axial X, monodentate succinate; axial OH, equatorial X, monodentate succinate; equatorial OH and X, bidentate succinate; axial OH, equatorial X, bidentate succinate; equatorial OH, axial X, bidentate succinate. The dashed blue

line corresponds to an estimated DLPNO/CBS energy. Hydrogen, carbon, nitrogen, oxygen, iron, and bromine are shown in white, gray, blue, red, brown, and maroon, respectively.

Next, we study the relative energetics of Fe(III)–OH isomers, because it has been suggested that isomerization of the Fe(III)–OH intermediate could selectively favor substrate halogenation over hydroxylation during the substrate rebound reaction, meaning that a species that was limited in its ability to isomerize would lead primarily to hydroxylated products in the absence of other selectivity-determining mechanisms.[58, 59] We find that the relative energetic ordering of most Fe(III)–OH isomers is consistent across all halides with small energetic differences of ca. 1 kcal/mol for some isomers as a result of slightly different optimized geometries (Figure 2 and Supporting Information Table S6 and Figure S5). The most stable bidentate succinate isomer with axial halide and equatorial OH is strongly preferred over monodentate isomers across all halides by ca. 5–9 kcal/mol (Figure 2). This suggests a potential difficulty in isomerization (see calculation of barriers in Sec. 4.3) of the most stable Fe(III)–OH isomer, implying that selective halogenation could be expected to take place only when the substrate is positioned more proximal to the halide by second-sphere interactions or the isomerization takes place prior to HAT.

Examination of optimized geometries of halide intermediates in their ground spin states shows that iron–halide bond lengths increase on average with halide size from 1.81 Å (F) to 2.25 Å (Cl) to 2.41 Å (Br) in Fe(IV)=O and Fe(III)–OH intermediates (Supporting Information Table S7). To assess whether this increase in bond lengths is solely due to differences in the size of the halides, we considered bond lengths scaled by the covalent radii of participating atoms (Supporting Information Table S8). The scaled Fe–F bond is shorter than Fe–Cl (0.84 vs 0.90), while scaled Fe–Cl and Fe–Br bond lengths are comparable. The shorter scaled and unscaled Fe–F bonds suggest that it would be harder for the substrate to approach the halide in the oxo or hydroxo intermediates, which could explain the challenges with C–H fluorination. All other metal–ligand

bond lengths are mostly comparable across fluoride, chloride, and bromide intermediates (Supporting Information Table S7). The Fe–Cl and Fe–Br distances observed in optimized geometries of Fe(II)–H_2O intermediates, i.e., 2.38 Å and 2.54 Å, respectively, are roughly comparable to those observed in the crystal structures of BesD and SyrB2, suggesting that the shortened Fe–F bond lengths are treated reliably by DFT (Supporting Information Table S9).

We next examine the binding strength of ligands to Fe as quantified through the Mayer bond order to understand how the differences in binding of monodentate and bidentate succinate to Fe relate to their energetic stabilities in oxo and hydroxo intermediates. Consistent with prior work on intermediates with chloride,[61] bidentate succinate binds more strongly to Fe than monodentate succinate but not as strongly as the bidentate αKG for intermediates with fluoride and bromide (Figure 3). In general, binding strengths of succinate and αKG to Fe are slightly weaker in intermediates with fluoride compared to the larger chloride and bromide halides, both of which exhibit similar bond orders (Figure 3). However, for Fe(III)–O_2 intermediates, αKG binds more strongly to Fe when bromide/fluoride is in the active site compared to chloride, i.e., bond order of 1.40 vs 1.23 (Figure 3). For Fe(II)–H_2O intermediates with fluoride in the active site, the water molecule in the axial position can form a hydrogen bond (HB) with fluoride (Supporting Information Figure S6). We find that αKG binds more strongly to Fe in the isomer with a HB between water and fluoride than it does in the isomer without the HB, i.e., bond order of 0.57 vs 0.47 (Figure 3). Overall, binding strengths of ligands to Fe demonstrate limited dependence on the active site halide, with succinate and bidentate αKG displaying slightly stronger binding strengths for increasingly heavy halides (Figure 3). Thus, the overall reactivity and bonding should be qualitatively similar regardless of halide. The stronger binding of αKG to Fe in Fe(III)–O_2 intermediates of fluoride and bromide could suggest that oxidative decarboxylation to form

Fe(IV)=O with succinate ligand might be slightly more difficult for these halides compared to the native chloride species. Nevertheless, prior experimental results demonstrate that the oxidative decarboxylation step occurs in a fluoride-bound version of the engineered enzyme SadX as proficiently as in the case where chloride or bromide are bound[50]. Thus, we focused our reaction coordinate analysis on only the HAT and rebound steps.

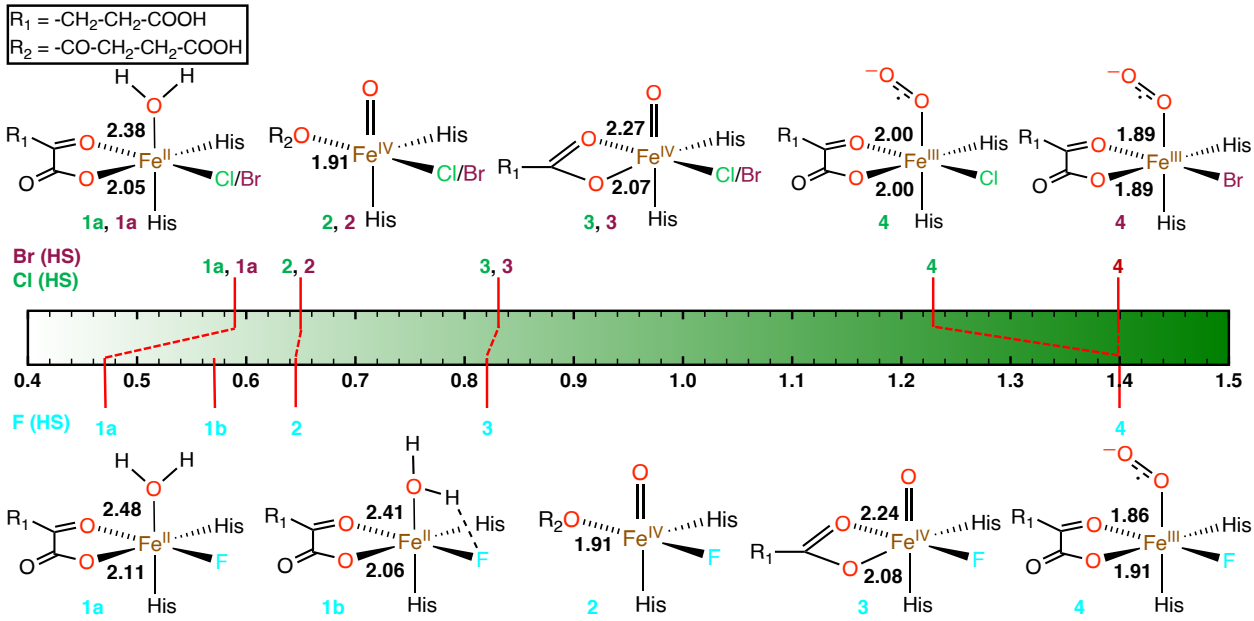

Figure 3. Scale demonstrating the Mayer bond orders of Fe–succinate/αKG bonds of ground state high-spin (HS) Fe intermediates with monodentate and bidentate succinate for three halides: (top) chloride and bromide, and (bottom) fluoride. The four intermediates shown are (1a) Fe(II)–H_2O with bidentate αKG without a hydrogen bond (HB) between water and halide, (1b) Fe(II)–H_2O with bidentate αKG with an HB between water and fluoride, (2) Fe(IV)=O with monodentate succinate, (3) Fe(IV)=O with bidentate succinate, and (4) Fe(III)–O_2 with bidentate αKG. The corresponding Fe–O (of succinate/αKG) bond lengths (in Å) are indicated in the insets.

4.2. HAT and Rebound Reaction Coordinates.

Non-heme iron halogenases are known to natively carry out C–H chlorination, as observed in SyrB2,[32] WelO5,[35] and BesD,[36] and SyrB2 has also been reported[32, 45] to carry out C–H bromination. In contrast, C–H fluorination has never been observed in non-heme iron halogenases. We study two reactions that are crucial for C–H halogenation for fluoride, chloride, and bromide

intermediates: the rate-determining HAT reaction and the competing rebound hydroxylation or halogenation reactions. We investigate HAT and rebound reactions to understand if differences across three halides for these reactions could explain why C–H chlorination or bromination are observed but fluorination is not observed. We study rebound of the substrate radical to both hydroxo and halide ligands and compare reaction energetics to understand how the preference for selective C–H hydroxylation vs halogenation differs across halides.

We model the HAT reactions using a bidentate succinate isomer with axial oxo and equatorial halide, which is the most stable isomer for the chloride Fe(IV)=O intermediate. While this is not the most stable isomer for fluoride or bromide intermediates, it is used for HAT reactions across all halides to enable consistent comparisons across halides and also because all bidentate succinate isomers are comparable in energy for the three halides (Figure 2). We find that the HAT reactions are accompanied by a significant reaction barrier (ca. 25 kcal/mol) for all halides suggesting that the nature of HAT is largely independent of the halide in the active site (Figure 4). This barrier height is in the middle range of those reported in prior work. Specifically, it is slightly lower than the HAT reaction barriers of ca. 30 kcal/mol observed for BesD in prior work[73] owing to additional constraints used in that study. In comparison to another study,[62] we find that the HAT barriers we observe are higher by ca. 5 kcal/mol, likely because we evaluate HAT reaction using first coordination sphere residues and a model substrate whereas first and second coordination sphere residues along with the complete substrate are used to compute HAT barrier in this other work. Additionally, the HAT barriers we observe in these non-heme halogenase models are comparable to those observed in non-heme hydroxylases such as TauD and non-heme demethylases[106, 107] with comparable O···H distances in transition states, as shown in prior computational work.[108-111] We also find that the hydroxo intermediate along with the substrate

radical formed after HAT are higher in energy by ca. 10–13 kcal/mol relative to the reactants, i.e., the oxo intermediate and substrate, across all three halides (Figure 4). The high-energy structures along the RCs observed at an O···H distance of 1.18 Å are confirmed to be transition states through Hessian calculations and the presence of a single imaginary frequency along the HAT RC (Figure 4 and Supporting Information Table S10). Furthermore, we obtained optimized geometries of these transition states along with the corresponding Hessian calculations with a single imaginary frequency along the HAT RC (Supporting Information Table S11 and Figure S7). The similar barriers experienced by all halide species indicate that differences in HAT are unlikely to lead to the lack of fluorination activity by non-heme iron halogenases. These observations are consistent with experimental work on engineered SadX variants that showed hydroxylation was accelerated in the presence of fluoride over other halides.[50]

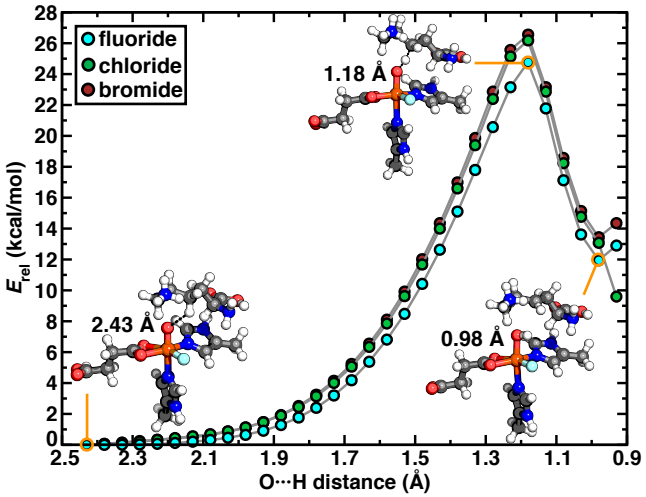

Figure 4. Relative hydrogen atom transfer (HAT) reaction energies (E_{rel}, in kcal/mol) for active sites with fluoride (shown in cyan), chloride (shown in green), and bromide (shown in maroon) ligands. Representative geometries of fluoride intermediates corresponding to minima and transition states are shown as insets. The O···H distance (in Å) between Fe(IV)=O and H of substrate is indicated as black dashed lines in the insets. Hydrogen, carbon, nitrogen, oxygen, fluorine, and iron are shown in white, gray, blue, red, cyan, and brown, respectively.

Next, we study rebound RCs in which the substrate radical reacts with hydroxo or halide ligands (Figure 1). Rebound reactions with hydroxo/halide are carried out using the most stable bidentate succinate isomers with axial hydroxo/halide, which are comparable in energy (Figure 2). Rebound reactions where the substrate radical rebounds to the hydroxo ligand are barrierless for larger halides, i.e., chloride and bromide but have a barrier of ca. 3 kcal/mol for the smaller fluoride intermediates (Figure 5). Rebound reactions where the substrate radical rebounds to the halide are barrierless for bromide and exhibit a minor barrier of ca. 1 kcal/mol for chloride (Figure 5). However, a significant barrier of 6.5 kcal/mol is observed for fluoride intermediates, suggesting that selective C–H fluorination could be challenging (Figure 5). The bulky model substrate along with the significantly shorter ·C···F distance (2.11 Å) in the transition state of the rebound reaction motivate us to investigate the extent to which the steric repulsion between the model substrate and the active site contributes to the observed barrier of 6.5 kcal/mol (Figure 5). We study the rebound reaction with a less bulky ethane model substrate and observe a significant barrier 8.8 kcal/mol, suggesting that the steric interactions between the substrate and active site models have little effect on the barrier for rebound to fluoride (Supporting Information Figure S8). Consistent with the Hammond-Leffler postulate[112, 113], the strong exothermicity corresponds to transition states that are much more similar to reactants than to the product rebound intermediate (Figure 5). The moderate to significant barriers for fluoride intermediates suggest that the rebound reaction could make C–H fluorination difficult in comparison to hydroxylation, consistent with prior work on SadX.[50] Additionally, we compute binding energies of Fe–X bonds (X = F, Cl, Br) and Fe–OH bond to understand the ease of rebound of the substrate radical to halogens or the hydroxo ligand (Supporting Information Table S12). We observe that the binding energies of larger halides, i.e., Cl and Br, to Fe are weaker which could further explain the ease of formation of chlorination and

brominated products (Supporting Information Table S12). However, Fe–F and Fe–OH bonds have comparable and much stronger bond dissociation energies (Supporting Information Table S12). The stronger bond dissociation of Fe–F bond combined with the significant rebound barrier could explain why we do not observe fluorinated products (Supporting Information Table S12).

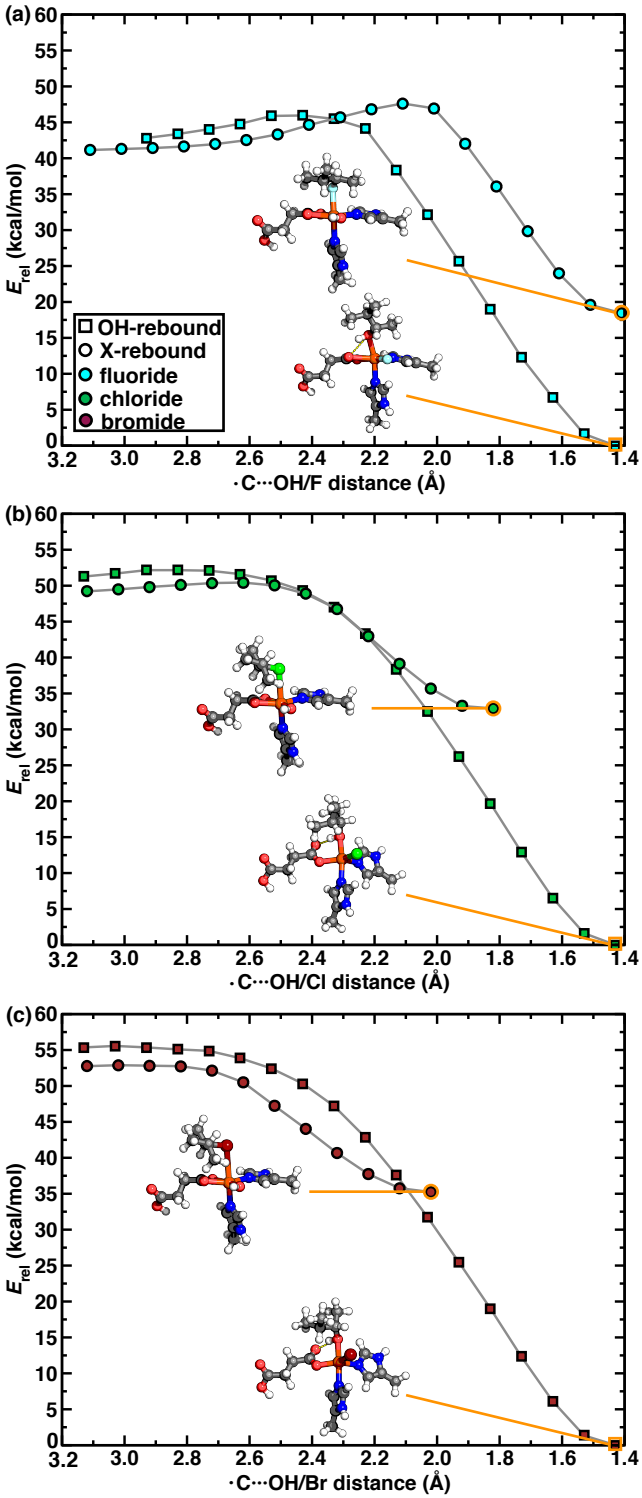

Figure 5. Reaction coordinates (RCs) for substrate radical rebound to hydroxo (OH, shown as squares) and halide (X, shown as circles) ligands for (a) fluoride (shown in cyan), (b) chloride (shown in green), and (c) bromide (shown in maroon) Fe(III)–OH intermediates. Geometries of rebound intermediates for all three halides are shown as insets. Hydrogen, carbon, nitrogen, oxygen, fluorine, chlorine, iron, and bromine are shown in white, gray, blue, red, cyan, green, brown, and maroon, respectively.

Further examination of rebound RCs reveals that the OH-rebound intermediates are energetically more favorable than halide-rebound intermediates for fluoride, chloride, and bromide intermediates, highlighting a greater thermodynamic driving force for hydroxylation (Figure 5). Thus, to avoid the hydroxylated product which could serve as a thermodynamic trap, enzymes must have chemical or structural strategies to favor halogenation over hydroxylation. For larger halides chloride and bromide, the OH-rebound intermediates are much more favorable than the halide-rebound intermediates by almost 35 kcal/mol, despite the fact that it is known that several enzymes do selectively brominate or chlorinate (Figure 5). Surprisingly, we observe that the OH-rebound intermediate is more stable than fluoride-rebound intermediate by a much smaller amount, ca. 18 kcal/mol (Figure 5). Despite the smaller energetic difference between OH-rebound and halide-rebound intermediates for fluoride relative to chloride/bromide, the higher barrier for rebound to fluoride could make C–H fluorination challenging compared to C–H chlorination or bromination (Figure 5 and Supporting Information Table S13).

4.3. Isomerization Barriers Between Fe(IV)=O and Fe(III)–OH Isomers Across Halides.

We next studied isomerization energy landscapes of Fe(IV)=O intermediates for all three halides to assess their likelihood of interconversion. We compare the active site isomerization across fluoride, chloride, and bromide intermediates to understand any differences in isomerization barriers and preferred orientation of oxo/halide ligands in intermediates of the catalytic cycle. We study two isomerization reaction coordinates (RCs) corresponding to the isomerization of a) halide and b) oxo ligands from axial to equatorial positions with both monodentate and bidentate succinate isomers. As previously discussed,[61] we expect isomerization of Fe(IV)=O intermediates to be favored when the active site has a monodentate succinate configuration to ensure the needed coordination flexibility within the active site to enable isomerization. Moreover, monodentate

metal-oxo isomers are only slightly less favorable than the bidentate isomers by ca. 3 kcal/mol (Figure 2).

We first study the isomerization RC that connects equatorial and axial halide isomers with equatorial oxo and monodentate succinate via an RC described by the N_{His}–Fe–X angle formed with the His ligand that is trans to the axial moiety (Figure 6). Comparison of this isomerization RC across three halides reveals differences in the stabilities of the equatorial halide configuration, which is not a minimum on the RC, but which we refer to as the equatorial isomer (Figure 4). This equatorial fluoride isomer is more favorable than the equatorial chloride and bromide isomers by ca. 2 kcal/mol and 3 kcal/mol, respectively (Figure 6). While the equatorial halide isomer is energetically more stable than the axial halide isomer for all three halides, their energies are more comparable for larger halides, i.e., the equatorial isomer is strongly preferred over the axial isomer by 4.5 kcal/mol for fluoride but only by 2.5 kcal/mol for bromide (Figure 6). We also find that the lowest-energy structure positions the halide tilted out of the equatorial plane and is observed at increasingly obtuse RC angles with increasing halide size, i.e., the lowest-energy N_{His}–Fe–X angle is 137°, 140°, and 147° in fluoride, chloride, and bromide intermediates, respectively (Figure 6). However, axial halide isomers are comparable in energy across all halides with axial fluoride and bromide isomers being slightly more stable than axial chloride isomer by ca. 1 kcal/mol (Figure 6). Overall, we expect that the differences in equatorial halide stabilities and halide-dependent N_{His}–Fe–X RC angle during isomerization could play a role in enabling C–H halogenation.

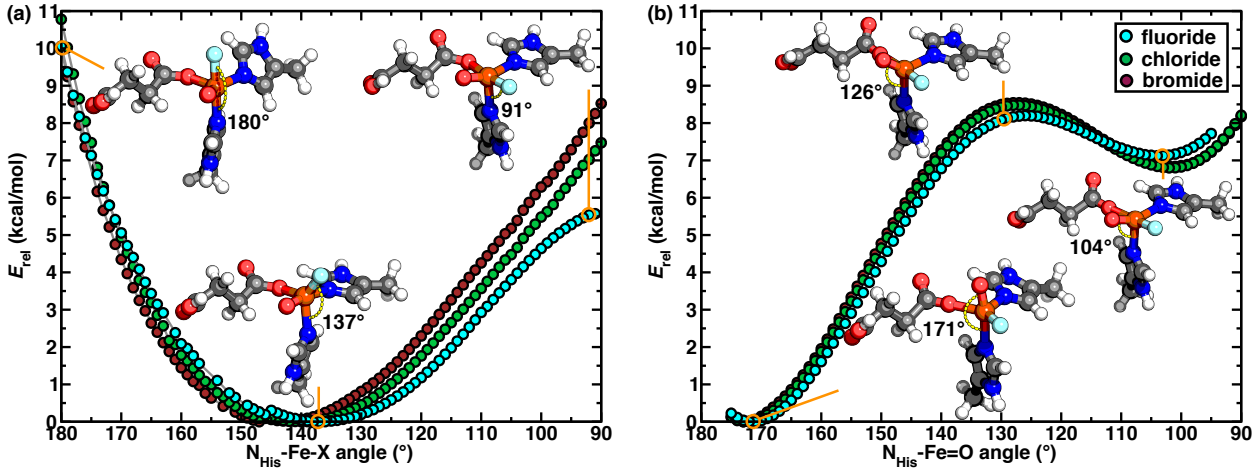

Figure 6. Reaction coordinates (RCs) for isomerization between (a) axial halide and equatorial halide, and (b) axial oxo and equatorial oxo with monodentate succinate for fluoride, chloride, and bromide Fe(IV)=O intermediates. Representative geometries of fluoride intermediates corresponding to minima and transition states are shown as insets. The N_{His}–Fe–F and N_{His}–Fe=O angles (in °) are indicated as yellow dashed curves in the insets. Hydrogen, carbon, nitrogen, oxygen, fluorine, and iron are shown in white, gray, blue, red, cyan, and brown, respectively.

The second RC corresponds to isomerization between the axial and equatorial positions for the oxo while the halide remains equatorial and succinate remains monodentate (Figure 6). We describe this RC as a function of N_{His}–Fe=O angle formed with the His ligand that is trans to the axial moiety (Figure 6). We find that the energies of both minima corresponding to axial oxo and equatorial oxo isomers differ by less than 1 kcal/mol between the smaller fluoride and larger chloride/bromide intermediates (Figure 6). Furthermore, the angular RCs are broadly consistent across all halides with a barrier of ca. 8 kcal/mol for oxo isomerization (Figure 6). The high-energy structures along these RCs are confirmed to be transition states with a single imaginary frequency along the angular RC mode (Supporting Information Table S14).

Although isomerization may occur in the Fe(IV)=O intermediate, positioning the reactive moiety away from the substrate at the cost of more sluggish but selective halogenation, it could alternately occur after hydrogen abstraction but before the radical rebound step. We thus also

explore a similar isomerization RC that connects axial OH and equatorial OH where halide remains equatorial and succinate remains monodentate (Supporting Information Figure S9). This RC is captured by the change in N_{His}–Fe–OH angle with the His trans to the axial hydroxo (Supporting Information Figure S9). Consistent with oxo isomerization RCs, the hydroxo isomerization RCs are also comparable across all halides (Supporting Information Figure S9). However, while an axial oxo isomer is favored along the oxo isomerization RC, here we observe that a hydroxo intermediate where OH tilts away from the axial position (N_{His}–Fe–OH = 154°) is favored for all halides (Figure 6 and Supporting Information Figure S9). Comparable oxo and hydroxo isomerization energy landscapes suggest that the preferred isomers before and after hydrogen atom abstraction are consistent for all halides. This indicates that the difficulty with C–H fluorination could stem from differences in halide isomerization that distinguish the behavior of fluoride and chloride/bromide intermediates.

We next obtained isomerization RCs where succinate is forced to remain bidentate along the RC to isolate the restrictive effect of bidentate coordination on isomerization and compare it to the RCs obtained with monodentate succinate (Figure 7). While the bidentate succinate isomer is more favorable than monodentate isomer by only 3 kcal/mol as shown in free optimizations, the minima of RCs where monodentate or bidentate succinate are enforced further destabilize the monodentate RC by ca. 20 kcal/mol (Figures 2 and 7). As explained in prior work[61], enforcing the monodentate succinate constraint deforms the C–O^-–Fe angle formed by succinate with Fe to a much larger value (by ca. 47°) than the angle observed in free optimizations, destabilizing the monodentate RC. Consistent with prior work[61], while bidentate succinate is more stable than its monodentate counterpart, we find that isomerization may not be feasible with fully bidentate succinate geometries for any of the three halides (Figure 7). Comparison of isomerization RCs

obtained with bidentate and monodentate isomers reveals that the structures on the bidentate RC for fluoride are energetically more favorable than those for chloride/bromide by ca. 2–3 kcal/mol (Figure 7). While isomerization RCs of monodentate isomers are comparable for all halides, the additional stability of bidentate isomers for fluoride relative to chloride/bromide suggests difficulty in isomerization from bidentate to monodentate isomers for fluoride which could explain why C–H fluorination is not observed in non-heme Fe(II) enzymes (Figure 7).

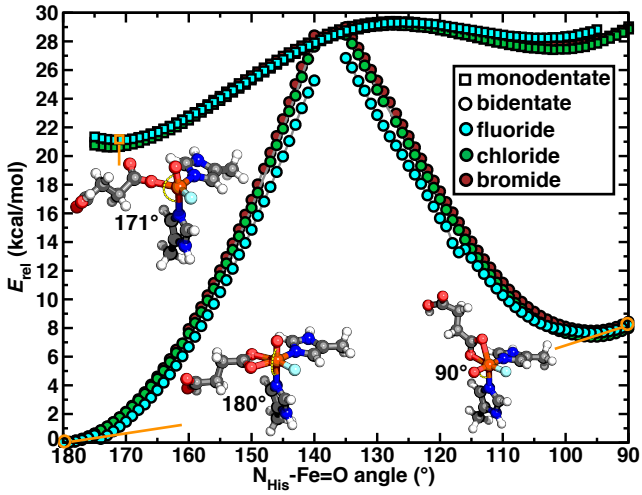

Figure 7. Reaction coordinates (RCs) for isomerization between axial oxo and equatorial oxo with bidentate succinate (shown as circles) and monodentate succinate (shown as squares) for fluoride (shown in cyan), chloride (shown in green), and bromide (shown in maroon) Fe(IV)=O intermediates. Representative geometries of fluoride intermediates corresponding to minima are shown as insets. The N_{His}–Fe=O angle (in °) is indicated as yellow dashed curves in the insets. Hydrogen, carbon, nitrogen, oxygen, fluorine, and iron are shown in white, gray, blue, red, cyan, and brown, respectively.

To further understand the contribution of the smaller size of fluoride to isomerization propensity, we obtained halide and oxo isomerization RCs of fluoride intermediates as single-point calculations of structures along isomerization RCs of chloride/bromide intermediates and vice-versa (Supporting Information Figures S10–S11). Study of these RCs obtained with both monodentate succinate and bidentate succinate helps us isolate the role of differences in shorter

(i.e., Fe–F) and longer (i.e., Fe–Cl/Br) bonds in isomerization (Supporting Information Figures S10–S11). Isomerization RCs of chloride/bromide intermediates obtained as single-point calculations at fluoride geometries are found to have higher barriers of ca. 2–3 kcal/mol when Fe–Cl/Br bonds are constrained to the shorter Fe–F bond lengths (Supporting Information Figure S10). On the contrary, isomerization RCs of fluoride intermediates obtained as single-point calculations at chloride/bromide geometries exhibit comparable or even slightly reduced barriers when the Fe–F bond is lengthened (Supporting Information Figure S10–S11). These observations suggest that targeted modifications to residues in the enzyme active site to introduce residues that form halogen bonds with fluoride or create local electric fields that elongate Fe–F bond lengths could make selective C–H fluorination more favorable. This longer Fe–F bond would then be expected to make the isomerization and rearrangement of the fluoride proximal to the substrate radical more favorable.

5. Conclusions.

While non-heme iron halogenases are known to carry out C–H chlorination and bromination, C–H fluorination activity has never been observed in these enzymes. We showed through a combination of DFT and WFT that there are significant differences between the smaller fluoride and the larger chloride/bromide intermediates in terms of their structural and energetic preferences. These studies which are carried out using only the first coordination sphere residues are found to differ slightly from a few prior studies that considered second coordinate sphere effects. While HAT reactions were found to be comparable for all three halides, we observed crucial differences in radical rebound reaction barriers for fluoride relative to chloride/bromide intermediates. The larger halide-rebound reaction barriers for fluoride intermediates in comparison to chloride/bromide intermediates could explain the challenges of C–H fluorination relative to C–

H chlorination and bromination.

Isomerization is expected to play a role in reaction selectivity in non-heme iron halogenases. We found that while chloride and bromide Fe(IV)=O intermediates have readily stabilized monodentate succinate isomers, fluoride monodentate isomers collapse back to bidentate structures, suggesting additional interactions with the greater protein environment might be necessary to enable the formation of this isomer for fluoride intermediates. Furthermore, we find that the much shorter Fe–F bonds relative to Fe–Cl/Fe–Br bonds suggest difficulty in the substrate approaching the oxo or hydroxo intermediates which could explain why C–H fluorination is challenging.

To further distinguish across all three halide intermediates, we studied active site isomerization of monodentate Fe(IV)=O between equatorial and axial halide isomers and observed differences in equatorial halide stabilities and the halide-dependent N_{His}–Fe–X RC angle during isomerization, which could play a role in C–H halogenation. We also found that bidentate isomers have additional stability for fluoride relative to chloride/bromide intermediates, suggesting difficulty in isomerization between bidentate and monodentate isomers for fluoride, which could explain why C–H fluorination is not observed in non-heme iron halogenases. To understand the effect of size differences, we obtained isomerization RCs of chloride/bromide intermediates with Fe–Cl and Fe–Br bonds constrained to shorter bond lengths that revealed increased reaction barriers. Conversely, fluoride RCs where Fe–F bond was elongated resulted in slightly reduced barriers suggesting that targeted modifications in the enzyme active site to position residues nearby that can form halogen bonds with fluoride and elongate Fe–F bonds could make selective C–H fluorination possible.

Overall, our study highlights the differences between the smaller fluoride and the larger chloride/bromide intermediates that could explain why selective C–H fluorination is not observed in non-heme iron halogenases. The differences in Fe–halide bond lengths and radical rebound reactions described in this work set the stage for further studies about targeted modifications of the enzyme active site to enable favorable C–H fluorination in non-heme iron halogenases.

ASSOCIATED CONTENT

Supporting Information. Extracted active site of WelO5 with three halides, i.e., F, Cl, Br; active site isomers and constrained atoms, angles, and distances; differences between implicit solvent and gas-phase metal-ligand bond lengths; potential spin states of active site intermediates with three halides (F, Cl, Br); tight PNO thresholds used in DLPNO-CCSD(T)/CBS calculations; active site isomers of intermediates formed during catalytic cycle; DLPNO-CCSD(T)/CBS spin-splitting energies of oxo and OH intermediates; differences between high-spin and low-spin metal-ligand bond lengths; relative energies of isomers obtained with DLPNO-CCSD(T)/CBS; optimized geometries of Fe(IV)=O isomers with three halides (F, Cl, Br); optimized geometries of Fe(III)–OH isomers with three halides (F, Cl, Br); optimized metal-ligand bond lengths of all active site isomers; covalent radii of fluorine, chlorine, iron, and bromine atoms; Fe–Cl and Fe–Br bond lengths in optimized geometries and crystal structures; optimized geometries of Fe(II)–H_2O and Fe(III)–O_2 isomers; N_{His}–Fe=O angles in transition state geometries along isomerization RC; RC for isomerization between axial and equatorial hydroxo; relaxed RCs and RCs obtained as single-points along relaxed RCs; O···H distances in high-energy structures along HAT RCs; O···H distances in optimized transition state geometries along HAT RCs; optimized geometries of transition states along HAT RCs; RC for ethane substrate radical rebound to fluoride ligand; binding energies of halides and hydroxo to Fe in Fe(III)–OH intermediates; relative energetics of halide-rebound and hydroxo-rebound intermediates (PDF)

Initial geometries, gas-phase optimized geometries, and solvent-phase optimized geometries of isomers of active site intermediates for all three halides, i.e., fluoride, chloride, and bromide; initial and optimized geometries along isomerization reaction coordinates for axial and equatorial oxo isomerization as well as axial and equatorial halide isomerization for fluoride, chloride, and bromide intermediates (ZIP)

AUTHOR INFORMATION

Corresponding Author

*email:hjkulik@mit.edu

Notes

The authors declare no competing financial interest.

ACKNOWLEDGMENT

This work was supported by the National Science Foundation under grant numbers CBET-1704266 and CBET-1846426. The authors acknowledge the MIT SuperCloud and Lincoln Laboratory Supercomputing Center for providing HPC resources that have contributed to the research results reported within this paper. This work also made use of Department of Defense HPCMP computing resources. This work was also carried out in part using computational resources from the Extreme Science and Engineering Discovery Environment (XSEDE), which is supported by National Science Foundation grant number ACI-1548562. H.J.K. holds a Career Award at the Scientific Interface from the Burroughs Wellcome Fund, an AAAS Marion Milligan Mason Award, and an Alfred P. Sloan Fellowship in Chemistry, which supported this work. The authors acknowledge Akash Bajaj, Aditya Nandy, Azadeh Nazemi, and Adam H. Steeves for providing critical readings of the manuscript.

References

(1) Karimov, R. R.; Hartwig, J. F. Transition-Metal-Catalyzed Selective Functionalization of C(sp(3))-H Bonds in Natural Products. *Angew. Chem., Int. Ed.* **2018**, *57* (16), 4234-4241.
(2) Brady, P. B.; Bhat, V. Recent Applications of Rh- and Pd-Catalyzed C(sp(3))-H Functionalization in Natural Product Total Synthesis. *Eur. J. Org. Chem.* **2017**, *2017* (35), 5179-5190.
(3) Sinha, S. K.; Zanoni, G.; Maiti, D. Natural Product Synthesis by C-H Activation. *Asian J. Org. Chem.* **2018**, *7* (7), 1178-1192.
(4) Yamaguchi, J.; Yamaguchi, A. D.; Itami, K. C-H Bond Functionalization: Emerging Synthetic Tools for Natural Products and Pharmaceuticals. *Angew. Chem., Int. Ed.* **2012**, *51* (36), 8960-9009.
(5) Chen, D. Y. K.; Youn, S. W. C-H Activation: A Complementary Tool in the Total Synthesis of Complex Natural Products. *Chem. - Eur. J.* **2012**, *18* (31), 9452-9474.
(6) Nandy, A.; Adamji, H.; Kastner, D. W.; Vennelakanti, V.; Nazemi, A.; Liu, M.; Kulik, H. J. Using Computational Chemistry to Reveal Nature's Blueprints for Single-Site Catalysis of C–H Activation. *ACS Catalysis* **2022**, *12*, 9281-9306.
(7) Nakama, Y.; Yoshida, O.; Yoda, M.; Araki, K.; Sawada, Y.; Nakamura, J.; Xu, S.; Miura, K.; Maki, H.; Arimoto, H. Discovery of a Novel Series of Semisynthetic Vancomycin Derivatives Effective against Vancomycin-Resistant Bacteria. *J. Med. Chem.* **2010**, *53* (6), 2528-2533.
(8) Gandeepan, P.; Muller, T.; Zell, D.; Cera, G.; Warratz, S.; Ackermann, L. 3d Transition Metals for C-H Activation. *Chem. Rev.* **2019**, *119* (4), 2192-2452.
(9) Chung, W.-j.; Vanderwal, C. D. Stereoselective Halogenation in Natural Product Synthesis. *Angew Chem Int Edit* **2016**, *55* (14), 4396-4434.
(10) Bucher, C.; Deans, R. M.; Burns, N. Z. Highly Selective Synthesis of Halomon, Plocamenone, and Isoplocamenone. *J. Am. Chem. Soc.* **2015**, *137* (40), 12784-12787.
(11) Dong, C.; Flecks, S.; Unversucht, S.; Haupt, C.; van Pee, K.-H.; Naismith, J. H. Tryptophan 7-Halogenase (PrnA) Structure Suggests a Mechanism for Regioselective Chlorination. *Science* **2005**, *309* (5744), 2216-2219.
(12) Latham, J.; Brandenburger, E.; Shepherd, S. A.; Menon, B. R. K.; Micklefield, J. Development of Halogenase Enzymes for Use in Synthesis. *Chem. Rev.* **2018**, *118* (1), 232-269.
(13) Blunt, J. W.; Copp, B. R.; Hu, W.-P.; Munro, M. H. G.; Northcote, P. T.; Prinsep, M. R. Marine Natural Products. *Natural Product Reports* **2009**, *26* (2), 170-244.
(14) Isanbor, C.; O'Hagan, D. Fluorine in Medicinal Chemistry: A Review of Anti-Cancer Agents. *J. Fluorine Chem.* **2006**, *127* (3), 303-319.
(15) Purser, S.; Moore, P. R.; Swallow, S.; Gouverneur, V. Fluorine in Medicinal Chemistry. *Chem. Soc. Rev.* **2008**, *37* (2), 320-330.
(16) Wang, J.; Sanchez-Rosello, M.; Acena, J. L.; del Pozo, C.; Sorochinsky, A. E.; Fustero, S.; Soloshonok, V. A.; Liu, H. Fluorine in Pharmaceutical Industry: Fluorine-Containing Drugs Introduced to the Market in the Last Decade (2001-2011). *Chem. Rev.* **2014**, *114* (4), 2432-2506.
(17) Song, S.; Li, X.; Wei, J.; Wang, W.; Zhang, Y.; Ai, L.; Zhu, Y.; Shi, X.; Zhang, X.; Jiao, N. DMSO-Catalysed Late-Stage Chlorination of (Hetero)Arenes. *Nat. Catal.* **2020**, *3* (2), 107-115.
(18) Gribble, G. W. Natural Organohalogens: A New Frontier for Medicinal Agents? *J. Chem. Educ.* **2004**, *81* (10), 1441-1449.
(19) Harris, C. M.; Kannan, R.; Kopecka, H.; Harris, T. M. The Role of the Chlorine Substituents in the Antibiotic Vancomycin - Preparation and Characterization of Monodechlorovancomycin and Didechlorovancomycin. *J. Am. Chem. Soc.* **1985**, *107* (23), 6652-6658.

(20) Jeschke, P. The Unique Role of Fluorine in the Design of Active Ingredients for Modern Crop Protection. *ChemBioChem* **2004**, *5* (5), 570-589.
(21) Jeschke, P. The Unique Role of Halogen Substituents in the Design of Modern Agrochemicals. *Pest Manage. Sci.* **2010**, *66* (1), 10-27.
(22) Timmins, A.; de Visser, S. P. A Comparative Review on the Catalytic Mechanism of Nonheme Iron Hydroxylases and Halogenases. *Catalysts* **2018**, *8* (8), 314.
(23) Blasiak, L. C.; Drennan, C. L. Structural Perspective on Enzymatic Halogenation. *Acc. Chem. Res.* **2009**, *42* (1), 147-155.
(24) Hausinger, R. P. Fe(II)/alpha-Ketoglutarate-Dependent Hydroxylases and Related Enzymes. *Critical Reviews in Biochemistry and Molecular Biology* **2004**, *39* (1), 21-68.
(25) Solomon, E. I.; Light, K. M.; Liu, L. V.; Srnec, M.; Wong, S. D. Geometric and Electronic Structure Contributions to Function in Non-Heme Iron Enzymes. *Acc. Chem. Res.* **2013**, *46* (11), 2725-2739.
(26) Costas, M.; Mehn, M. P.; Jensen, M. P.; Que Jr, L. Dioxygen Activation at Mononuclear Nonheme Iron Active Sites: Enzymes, Models, and Intermediates. *Chem. Rev.* **2004**, *104* (2), 939-986.
(27) Krebs, C.; Fujimori, D. G.; Walsh, C. T.; Bollinger, J. M. Non-Heme Fe(IV)-Oxo Intermediates. *Acc. Chem. Res.* **2007**, *40* (7), 484-492.
(28) Vaillancourt, F. H.; Yeh, E.; Vosburg, D. A.; O'connor, S. E.; Walsh, C. T. Cryptic Chlorination by a Non-Haem Iron Enzyme During Cyclopropyl Amino Acid Biosynthesis. *Nature* **2005**, *436* (7054), 1191.
(29) Khare, D.; Wang, B.; Gu, L.; Razelun, J.; Sherman, D. H.; Gerwick, W. H.; Håkansson, K.; Smith, J. L. Conformational Switch Triggered by α-Ketoglutarate in a Halogenase of Curacin A Biosynthesis. *Proc. Natl. Acad. Sci. U. S. A.* **2010**, *107* (32), 14099-14104.
(30) Pratter, S. M.; Light, K. M.; Solomon, E. I.; Straganz, G. D. The Role of Chloride in the Mechanism of O2 Activation at the Mononuclear Nonheme Fe (II) Center of the Halogenase HctB. *J. Am. Chem. Soc.* **2014**, *136* (26), 9385-9395.
(31) Vaillancourt, F. H.; Yin, J.; Walsh, C. T. SyrB2 in Syringomycin E Biosynthesis is a Nonheme FeII α-Ketoglutarate- and O2-Dependent Halogenase. *Proc. Natl. Acad. Sci. U. S. A.* **2005**, *102* (29), 10111-10116.
(32) Blasiak, L. C.; Vaillancourt, F. H.; Walsh, C. T.; Drennan, C. L. Crystal Structure of the Non-Haem Iron Halogenase SyrB2 in syringomycin Biosynthesis. *Nature* **2006**, *440* (7082), 368-371.
(33) Galonic, D. P.; Barr, E. W.; Walsh, C. T.; Bollinger, J. M.; Krebs, C. Two Interconverting Fe((IV)) Intermediates in Aliphatic Chlorination by the Halogenase CytC3. *Nat. Chem. Biol.* **2007**, *3* (2), 113-116.
(34) Wong, C.; Fujimori, D. G.; Walsh, C. T.; Drennan, C. L. Structural Analysis of an Open Active Site Conformation of Nonheme Iron Halogenase CytC3. *J. Am. Chem. Soc.* **2009**, *131* (13), 4872-4879.
(35) Mitchell, A. J.; Zhu, Q.; Maggiolo, A. O.; Ananth, N. R.; Hillwig, M. L.; Liu, X.; Boal, A. K. Structural Basis for Halogenation by Iron- and 2-oxo-glutarate-dependent Enzyme WelO5. *Nat. Chem. Biol.* **2016**, *12* (8), 636-640.
(36) Neugebauer, M. E.; Sumida, K. H.; Pelton, J. G.; McMurry, J. L.; Marchand, J. A.; Chang, M. C. Y. A Family of Radical Halogenases for the Engineering of Amino-Acid-Based Products. *Nat. Chem. Biol.* **2019**, *15* (10), 1009-1016.
(37) Price, J. C.; Barr, E. W.; Glass, T. E.; Krebs, C.; Bollinger, J. M. Evidence for Hydrogen Abstraction from C1 of Taurine by the High-Spin Fe(IV) Intermediate Detected during Oxygen

Activation by Taurine :alpha-Ketoglutarate Dioxygenase (TauD). *J. Am. Chem. Soc.* **2003**, *125* (43), 13008-13009.
(38) Price, J. C.; Barr, E. W.; Tirupati, B.; Bollinger, J. M.; Krebs, C. The First Direct Characterization of a High-Valent Iron Intermediate in the Reaction of an alpha-Ketoglutarate-Dependent Dioxygenase: A High-Spin Fe(IV) Complex in Taurine/alpha-Ketoglutarate Dioxygenase (TauD) from Escherichia coli. *Biochemistry* **2003**, *42* (24), 7497-7508.
(39) Martinez, S.; Hausinger, R. P. Catalytic Mechanisms of Fe(II)-and 2-Oxoglutarate-dependent Oxygenases. *J. Biol. Chem.* **2015**, *290* (34), 20702-20711.
(40) Koehntop, K. D.; Emerson, J. P.; Que, L. The 2-His-1-Carboxylate Facial Triad: A Versatile Platform for Dioxygen Activation by Mononuclear Non-Heme Iron(II) Enzymes. *J. Biol. Inorg. Chem.* **2005**, *10* (2), 87-93.
(41) Hegg, E. L.; Que, L. The 2-His-1-Carboxylate Facial Triad - An Emerging Structural Motif in Mononuclear Non-Heme Iron(II) Enzymes. *Eur. J. Biochem.* **1997**, *250* (3), 625-629.
(42) Que, L. One Motif - Many Different Reactions. *Nat. Struct. Biol.* **2000**, *7* (3), 182-184.
(43) Prakash, G. K. S.; Mathew, T.; Hoole, D.; Esteves, P. M.; Wang, Q.; Rasul, G.; Olah, G. A. N-Halosuccinimide/BF3-H2O, Efficient Electrophilic Halogenating Systems for Aromatics. *J. Am. Chem. Soc.* **2004**, *126* (48), 15770-15776.
(44) Altus, K. M.; Love, J. A. The Continuum of Carbon-Hydrogen (C-H) Activation Mechanisms and Terminology. *Communications Chemistry* **2021**, *4* (1), 173.
(45) Vaillancourt, F. H.; Vosburg, D. A.; Walsh, C. T. Dichlorination and Bromination of a Threonyl-S-Carrier Protein by the Non-Heme Fe-II Halogenase SyrB2. *ChemBioChem* **2006**, *7* (5), 748-752.
(46) Agarwal, V.; Miles, Z. D.; Winter, J. M.; Eustaquio, A. S.; El Gamal, A. A.; Moore, B. S. Enzymatic Halogenation and Dehalogenation Reactions: Pervasive and Mechanistically Diverse. *Chem. Rev.* **2017**, *117* (8), 5619-5674.
(47) Gribble, G. W. The Natural Production of Organobromine Compounds. *Environ. Sci. Pollut. Res.* **2000**, *7* (1), 37-49.
(48) Vaillancourt, F. H.; Yeh, E.; Vosburg, D. A.; Garneau-Tsodikova, S.; Walsh, C. T. Nature's Inventory of Halogenation Catalysts: Oxidative Strategies Predominate. *Chem. Rev.* **2006**, *106* (8), 3364-3378.
(49) Lohman, D. C.; Edwards, D. R.; Wolfenden, R. Catalysis by Desolvation: The Catalytic Prowess of SAM-Dependent Halide-Alkylating Enzymes. *J. Am. Chem. Soc.* **2013**, *135* (39), 14473-14475.
(50) Chan, N. H.; Gomez, C. A.; Vennelakanti, V.; Du, Q.; Kulik, H. J.; Lewis, J. C. Non-Native Anionic Ligand Binding and Reactivity in Engineered Variants of the Fe(II)- and alpha-Ketoglutarate-Dependent Oxygenase, SadA. *Inorg. Chem.* **2022**, *61* (36), 14477-14485.
(51) Gerard, E. F.; Yadav, V.; Goldberg, D. P.; de Visser, S. P. What Drives Radical Halogenation versus Hydroxylation in Mononuclear Nonheme Iron Complexes? A Combined Experimental and Computational Study. *J. Am. Chem. Soc.* **2022**, *144* (24), 10752-10767.
(52) Inoue, M.; Sumii, Y.; Shibata, N. Contribution of Organofluorine Compounds to Pharmaceuticals. *ACS Omega* **2020**, *5* (19), 10633-10640.
(53) Ilardi, E. A.; Vitaku, E.; Njardarson, J. T. Data-Mining for Sulfur and Fluorine: An Evaluation of Pharmaceuticals To Reveal Opportunities for Drug Design and Discovery. *J. Med. Chem.* **2014**, *57* (7), 2832-2842.
(54) Gillis, E. P.; Eastman, K. J.; Hill, M. D.; Donnelly, D. J.; Meanwell, N. A. Applications of Fluorine in Medicinal Chemistry. *J. Med. Chem.* **2015**, *58* (21), 8315-8359.

(55) Lin, A.; Huehls, C. B.; Yang, J. Recent Advances in C-H Fluorination. *Org. Chem. Front.* **2014**, *1* (4), 434-438.
(56) Wong, S. D.; Srnec, M.; Matthews, M. L.; Liu, L. V.; Kwak, Y.; Park, K.; Bell, C. B.; Alp, E. E.; Zhao, J.; Yoda, Y.; et al. Elucidation of the Fe(IV)=O Intermediate in the Catalytic Cycle of the Halogenase SyrB2. *Nature* **2013**, *499* (7458), 320-323.
(57) Martinie, R. J.; Livada, J.; Chang, W.-c.; Green, M. T.; Krebs, C.; Bollinger, J. M.; Silakov, A. Experimental Correlation of Substrate Position with Reaction Outcome in the Aliphatic Halogenase, SyrB2. *J. Am. Chem. Soc.* **2015**, *137* (21), 6912-6919.
(58) Borowski, T.; Noack, H.; Radon, M.; Zych, K.; Siegbahn, P. E. M. Mechanism of Selective Halogenation by SyrB2: A Computational Study. *J. Am. Chem. Soc.* **2010**, *132* (37), 12887-12898.
(59) Huang, J.; Li, C.; Wang, B.; Sharon, D. A.; Wu, W.; Shaik, S. Selective Chlorination of Substrates by the Halogenase SyrB2 Is Controlled by the Protein According to a Combined Quantum Mechanics/Molecular Mechanics and Molecular Dynamics Study. *ACS Catal.* **2016**, *6* (4), 2694-2704.
(60) Mehmood, R.; Qi, H. W.; Steeves, A. H.; Kulik, H. J. The Protein's Role in Substrate Positioning and Reactivity for Biosynthetic Enzyme Complexes: the Case of SyrB2/SyrB1. *ACS Catal.* **2019**, *9* (6), 4930-4943.
(61) Vennelakanti, V.; Mehmood, R.; Kulik, H. J. Are Vanadium Intermediates Suitable Mimics in Non-Heme Iron Enzymes? An Electronic Structure Analysis. *ACS Catal.* **2022**, *12* (9), 5489-5501.
(62) Li, R.-N.; Chen, S.-L. Mechanism for the Halogenation and Azidation of Lysine Catalyzed by Non-heme Iron BesD Enzyme. *Chem. - Asian J.* **2022**, *17* (17), e202200438.
(63) Groves, J. T. Key Elements of the Chemistry of Cytochrome-P-450 - the Oxygen Rebound Mechanism. *J. Chem. Educ.* **1985**, *62* (11), 928-931.
(64) Dong, C.; Huang, F.; Deng, H.; Schaffrath, C.; Spencer, J. B.; O'Hagan, D.; Naismith, J. H. Crystal Structure and Mechanism of a Bacterial Fluorinating Enzyme. *Nature* **2004**, *427* (6974), 561-565.
(65) Huang, S.; Ma, L.; Tong, M. H.; Yu, Y.; O'Hagan, D.; Deng, H. Fluoroacetate Biosynthesis from the Marine-Derived Bacterium Streptomyces xinghaiensis NRRL B-24674. *Organic & Biomolecular Chemistry* **2014**, *12* (27), 4828-4831.
(66) Cheng, X.; Ma, L. Enzymatic Synthesis of Fluorinated Compounds. *Appl. Microbiol. Biotechnol.* **2021**, *105* (21-22), 8033-8058.
(67) O'Hagan, D.; Schaffrath, C.; Cobb, S. L.; Hamilton, J. T. G.; Murphy, C. D. Biosynthesis of an Organofluorine Molecule - A Fluorinase Enzyme has been Discovered that Catalyses Carbon-Fluorine Bond Formation. *Nature* **2002**, *416* (6878), 279-279.
(68) Cowdrey, W. A.; Hughes, E. D.; Ingold, C. K.; Masterman, S.; Scott, A. D. Reaction Kinetics and the Walden Inversion Part VI Relation of Steric Orientation to Mechanism in Substitution involving Halogen Atoms and Simple or Substituted Hydroxyl Groups. *J. Chem. Soc.* **1937**, (0), 1252-1271.
(69) Olmstead, W. N.; Brauman, J. I. Gas-Phase Nucleophilic Displacement-Reactions. *J. Am. Chem. Soc.* **1977**, *99* (13), 4219-4228.
(70) Manikandan, P.; Zhang, J.; Hase, W. L. Chemical Dynamics Simulations of X- + CH3Y -> XCH3 + Y- Gas-Phase S(N)2 Nucleophilic Substitution Reactions. Nonstatistical Dynamics and Nontraditional Reaction Mechanisms. *J. Phys. Chem. A* **2012**, *116* (12), 3061-3080.
(71) Yang, Z.-Z.; Li, X. Ion Solvation in Water from Molecular Dynamics Simulation with the ABEEM/MM Force Field. *J. Phys. Chem. A* **2005**, *109* (16), 3517-3520.

(72) Eason, C. Sodium Monofluoroacetate (1080) Risk Assessment and Risk Communication. *Toxicology* **2002**, *181-182*, 523-530.
(73) Kastner, D. W.; Nandy, A.; Mehmood, R.; Kulik, H. J. Mechanistic Insights Into Substrate Positioning Across Non-heme Fe(II)/a-ketoglutarate-dependent Halogenases and Hydroxylases. *ACS Catalysis* **2023**, *13*, 2489-2501.
(74) Mehmood, R.; Vennelakanti, V.; Kulik, H. J. Spectroscopically Guided Simulations Reveal Distinct Strategies for Positioning Substrates to Achieve Selectivity in Nonheme Fe(II)/α-Ketoglutarate-Dependent Halogenases. *ACS Catal.* **2021**, *11* (19), 12394–12408.
(75) Matthews, M. L.; Neumann, C. S.; Miles, L. A.; Grove, T. L.; Booker, S. J.; Krebs, C.; Walsh, C. T.; Bollinger Jr, J. M. Substrate positioning controls the partition between halogenation and hydroxylation in the aliphatic halogenase, SyrB2. *Proceedings of the National Academy of Sciences* **2009**, *106* (42), 17723-17728.
(76) Kulik, H. J.; Drennan, C. L. Substrate Placement Influences Reactivity in Non-heme Fe (II) Halogenases and Hydroxylases. *Journal of Biological Chemistry* **2013**, *288*, 11233–11241.
(77) Hillwig, M. L.; Fuhrman, H. A.; Ittiamornkul, K.; Sevco, T. J.; Kwak, D. H.; Liu, X. Identification and Characterization of a Welwitindolinone Alkaloid Biosynthetic Gene Cluster in the Stigonematalean Cyanobacterium Hapalosiphon welwitschii. *ChemBioChem* **2014**, *15* (5), 665-669.
(78) Hillwig, M. L.; Liu, X. A New Family of Iron-Dependent Halogenases Acts on Freestanding Substrates. *Nat. Chem. Biol.* **2014**, *10* (11), 921-923.
(79) Ioannidis, E. I.; Gani, T. Z. H.; Kulik, H. J. molSimplify: A Toolkit for Automating Discovery in Inorganic Chemistry. *J. Comput. Chem.* **2016**, *37* (22), 2106-2117.
(80) O'Boyle, N. M.; Morley, C.; Hutchison, G. R. Pybel: A Python Wrapper for the OpenBabel Cheminformatics Toolkit. *Chem. Cent. J.* **2008**, *2*, 5.
(81) O'Boyle, N. M.; Banck, M.; James, C. A.; Morley, C.; Vandermeersch, T.; Hutchison, G. R. Open Babel: An Open Chemical Toolbox. *J. Cheminf.* **2011**, *3*, 33.
(82) Hanwell, M. D.; Curtis, D. E.; Lonie, D. C.; Vandermeersch, T.; Zurek, E.; Hutchison, G. R. Avogadro: An Advanced Semantic Chemical Editor, Visualization, and Analysis Platform. *J. Cheminf.* **2012**, *4*, 17.
(83) Rappe, A. K.; Casewit, C. J.; Colwell, K. S.; Goddard, W. A. I.; Skiff, W. M. UFF, a Full Periodic-Table Force-Field for Molecular Mechanics and Molecular-Dynamics Simulations. *J. Am. Chem. Soc.* **1992**, *114* (25), 10024-10035.
(84) Neese, F. Software Update: The ORCA Program System, Version 4.0. *Wiley Interdiscip. Rev.: Comput. Mol. Sci.* **2018**, *8* (1).
(85) Adamo, C.; Barone, V. Toward Reliable Density Functional Methods Without Adjustable Parameters: The PBE0 Model. *J. Chem. Phys.* **1999**, *110* (13), 6158-6170.
(86) Weigend, F.; Ahlrichs, R. Balanced Basis Sets of Split Valence, Triple Zeta Valence and Quadruple Zeta Valence Quality for H to Rn: Design and Assessment of Accuracy. *Phys. Chem. Chem. Phys.* **2005**, *7* (18), 3297-3305.
(87) Grimme, S.; Antony, J.; Ehrlich, S.; Krieg, H. A Consistent and Accurate ab initio Parametrization of Density Functional Dispersion Correction (DFT-D) for the 94 Elements H-Pu. *J. Chem. Phys.* **2010**, *132* (15), 154104.
(88) Grimme, S.; Ehrlich, S.; Goerigk, L. Effect of the Damping Function in Dispersion Corrected Density Functional Theory. *J. Comput. Chem.* **2011**, *32* (7), 1456-1465.
(89) Baerends, E. J.; Ellis, D. E.; Ros, P. Self-Consistent Molecular Hartree-Fock-Slater Calculations - I. The Computational Procedure. *Chem. Phys.* **1973**, *2* (1), 41-51.

(90) Whitten, J. L. Coulombic Potential-Energy Integrals and Approximations. *J. Chem. Phys.* **1973**, *58* (10), 4496-4501.
(91) Dunlap, B. I.; Connolly, J. W. D.; Sabin, J. R. On Some Approximations in Applications of Xα Theory. *J. Chem. Phys.* **1979**, *71* (8), 3396.
(92) Eichkorn, K.; Weigend, F.; Treutler, O.; Ahlrichs, R. Auxiliary Basis Sets for Main Row Atoms and Transition Metals and Their Use to Approximate Coulomb Potentials. *Theor. Chem. Acc.* **1997**, *97* (1-4), 119-124.
(93) Kendall, R. A.; Fruchtl, H. A. The Impact of the Resolution of the Identity Approximate Integral Method on Modern Ab Initio Algorithm Development. *Theor. Chem. Acc.* **1997**, *97* (1-4), 158-163.
(94) Stoychev, G. L.; Auer, A. A.; Neese, F. Automatic Generation of Auxiliary Basis Sets. *J. Chem. Theory Comput.* **2017**, *13* (2), 554-562.
(95) Barone, V.; Cossi, M. Quantum Calculation of Molecular Energies and Energy Gradients in Solution by a Conductor Solvent Model. *J. Phys. Chem. A* **1998**, *102* (11), 1995-2001.
(96) Riplinger, C.; Neese, F. An Efficient and Near Linear Scaling Pair Natural Orbital Based Local Coupled Cluster Method. *J. Chem. Phys.* **2013**, *138* (3), 034106.
(97) Riplinger, C.; Sandhoefer, B.; Hansen, A.; Neese, F. Natural Triple Excitations in Local Coupled Cluster Calculations with Pair Natural Orbitals. *J. Chem. Phys.* **2013**, *139* (13), 134101.
(98) Zhong, S.; Barnes, E. C.; Petersson, G. A. Uniformly Convergent n-tuple-zeta Augmented Polarized (nZaP) Basis Sets for Complete Basis Set Extrapolations. I. Self-Consistent Field Energies. *J. Chem. Phys.* **2008**, *129* (18), 184116.
(99) Neese, F.; Valeev, E. F. Revisiting the Atomic Natural Orbital Approach for Basis Sets: Robust Systematic Basis Sets for Explicitly Correlated and Conventional Correlated ab initio Methods? *J. Chem. Theory Comput.* **2011**, *7* (1), 33-43.
(100) Helgaker, T.; Klopper, W.; Koch, H.; Noga, J. Basis-Set Convergence of Correlated Calculations on Water. *J. Chem. Phys.* **1997**, *106* (23), 9639-9646.
(101) Lu, T.; Chen, F. Multiwfn: A Multifunctional Wavefunction Analyzer. *J. Comput. Chem.* **2012**, *33* (5), 580-592.
(102) Fujimori, D. G.; Barr, E. W.; Matthews, M. L.; Koch, G. M.; Yonce, J. R.; Walsh, C. T.; Bollinger, J. M.; Krebs, C.; Riggs-Gelasco, P. J. Spectroscopic Evidence for a High-Spin Br-Fe(IV)-Oxo Intermediate in the alpha-Ketoglutarate-Dependent Halogenase CytC3 from Streptomyces. *J. Am. Chem. Soc.* **2007**, *129* (44), 13408-13409.
(103) Purpero, V.; Moran, G. R. The Diverse and Pervasive Chemistries of the Alpha-Keto Acid Dependent Enzymes. *J. Biol. Inorg. Chem.* **2007**, *12* (5), 587-601.
(104) Mitchell, A. J.; Dunham, N. P.; Bergman, J. A.; Wang, B.; Zhu, Q.; Chang, W.-c.; Liu, X.; Boal, A. K. Structure-Guided Reprogramming of a Hydroxylase to Halogenate its Small Molecule Substrate. *Biochemistry* **2017**, *56* (3), 441-444.
(105) Matthews, M. L.; Krest, C. M.; Barr, E. W.; Vaillancourt, F. H.; Walsh, C. T.; Green, M. T.; Krebs, C.; Bollinger, J. M. Substrate-Triggered Formation and Remarkable Stability of the C-H Bond-Cleaving Chloroferryl Intermediate in the Aliphatic Halogenase, SyrB2. *Biochemistry* **2009**, *48* (20), 4331-4343.
(106) Rifayee, S. B. J. S.; Chaturvedi, S. S.; Warner, C.; Wildey, J.; White, W.; Thompson, M.; Schofield, C. J.; Christov, C. Z. Catalysis by KDM6 Histone Demethylases - A Synergy between the Non-Heme Iron(II) Center, Second Coordination Sphere, and Long-Range Interactions. *Chemistry - A European Journal* **2023**.

(107) Chaturvedi, S. S.; Ramanan, R.; Lehnert, N.; Schofield, C. J.; Karabencheva-Christova, T. G.; Christov, C. Z. Catalysis by the Non-Heme Iron(II) Histone Demethylase PHF8 Involves Iron Center Rearrangement and Conformational Modulation of Substrate Orientation. *ACS Catal.* **2020**, *10* (2), 1195-1209.
(108) Ye, S.; Neese, F. Nonheme Oxo-Iron(IV) Intermediates Form an Oxyl Radical upon Approaching the C-H Bond Activation Transition State. *Proc. Natl. Acad. Sci. U. S. A.* **2011**, *108* (4), 1228-1233.
(109) Janardanan, D.; Wang, Y.; Schyman, P.; Que, L.; Shaik, S. The Fundamental Role of Exchange-Enhanced Reactivity in C-H Activation by
=2 Oxo Iron(IV) Complexes. *Angew. Chem., Int. Ed.* **2010**, *49* (19), 3342-3345.
(110) de Visser, S. P. Propene Activation by the Oxo-Iron Active Species of Taurine/α-Ketoglutarate Dioxygenase (TauD) Enzyme. How Does the Catalysis Compare to Heme-Enzymes? *J. Am. Chem. Soc.* **2006**, *128* (30), 9813-9824.
(111) Ghafoor, S.; Mansha, A.; de Visser, S. P. Selective Hydrogen Atom Abstraction from Dihydroflavonol by a Nonheme Iron Center Is the Key Step in the Enzymatic Flavonol Synthesis and Avoids Byproducts. *J. Am. Chem. Soc.* **2019**, *141* (51), 20278-20292.
(112) Hammond, G. S. A Correlation of Reaction Rates. *J. Am. Chem. Soc.* **1955**, *77* (2), 334-338.
(113) Leffler, J. E. Parameters for the Description of Transition States. *Science* **1953**, *117* (3039), 340-341.